OPTIMUM LOCATION OF PRESSURE MEASURMENTS AROUND A WING AS A DYNAMIC CONTROL INPUT IN SMOOTH AND TURBULENT CONDITIONS

Matthew Marino*, Sridhar Ravi, Simon Watkins*****
***PhD Student, Royal Melbourne Institute of Technology, **Postdoc, University of Tuebingen, ***Professor of engineering, Royal Melbourne Institute of Technology**
matthew.marino@rmit.edu.au;sridhar.ravi@uni-tuebingen.de;simon@rmit.edu.au

Abstract

Smooth-flow low-Reynolds number experiments on wings have been fulfilled however the effects of free-stream turbulence on small fixed wing aircraft are relatively unknown. Experiments at low Reynolds number (approximately 140,000) where performed on a 1-meter span NACA2313 wing in a 3 x 2 x 9 meter wind tunnel. Experiments where conducted under relative smooth flow (Turbulence Intensity (TI) = 1.5%) and under elevated levels of free stream turbulence (TI = 7.2%, length scale = 0.23m) to evaluate the aerodynamic influence of free-stream turbulence. Turbulence generating grids were placed before tunnel contraction to induce appropriate flow mixing to replicate a turbulent flow condition similar to low altitude turbulence provoked from protruding ground objects in urban terrains. Dynamic pressures were measured through pressure taps manufactured into the NACA2313 wing at 4 span wise locations linking into a Dynamic Pressure Measurement System (DPMS). Time-averaged data displayed increased wing performance when tested under elevated levels of free stream turbulence. Angles off attack above stall revealed more flow attachment in comparison to smooth flow experiments. Time-averaged standard deviation of pressures revealed max pressure variance at the leading edge of the wing with variance decay as x/c increased. Flow separation (stall) increased standard deviation at all x/c locations suggesting regions of flow instability. Linear relationship was discovered between local chord-wise Cp at 14% and 17% of the suction and pressure surface of the wing respectively. High correlation co-efficient suggest acceptable levels of linearity allowing a single chord-wise pressure tap to be used to estimate integrated pressure.

1 Introduction

The function and application of current autopilot systems for the purpose of turbulence correction has been well researched and documented. Although current systems of active control has shown benefit in larger commercial and military aircraft alike, its application within low altitude unmanned vehicles has shown capability limitations when applying to most small UAV and MAV systems[1]. For surveillance missions a small UAV or MAV system is required to hold an acceptable level of steady level flight for successful video data acquisition[2]. Although smaller, lighter and more state of the are systems exist for MAV application[3], the level of assisted control for smooth flight within the Atmospheric Boundary Layer (ABL) is still regarded as unsatisfactory [4]. The common flight feedback system utilizes an IMU sensor and has been the primary sensoring device on past and current flight correction control systems[5]. This control method comprises of sensing inertial inflight perturbations and applying calculated control response to return the air vehicle to the steady level flight condition[3]. For commercial and military aircraft such a system would be adequate in reducing pilot load however for air vehicles acquiring video data, such a perturbation can reduce the amount and quality of video data acquired [6] with roll being the axis most affected to turbulence[7]. MAV research has developed flying vehicles less the

1-meter in span increasing the effects of turbulence in low altitude flight[7]. In some high turbulence scenarios, grounded MAV pilots have experienced difficulty avoiding collision and maintaining a steady and level flight path[8]. UAV and MAV control systems must offer a superior level of controlled response in various flight environments to allow for successful surveillance missions with diminutive collision and long periods of steady level flight for an array of flight environments.

Flying animals have shown controlled flight with the ability to takeoff, loiter and perch within high turbulence terrains such as city centers and forests [9]. Such flight characteristics have been assumed to be produced by various biological mechanisms in working in harmony[10]. Past literature has made reference to biological sensing devices allowing for flying animals to decide for optimum configuration within a flight terrain [11]. Observing animal flight has sparked research into various aspects of bird flight producing designs mimicking the biological mechanisms used by flying animals such as gull configurations, wing morphing and membrane wing designs[12]. This field of research allowed for inflight configuration changes however did not allow for reciprocal flapping or constant configuration change. Such flapping mechanisms require high energy sources to allow for constant mechanical flapping and does not allow for endurance times greater than 10 minutes[13]. Although bio mimicking flight devices has shown performance benefits in MAV flight, it is unknown if such devices have the ability to alleviate turbulence or offer an advantageous flight scenario to the common rigid wing design. Animal flight observation has also observed flying animals to have advanced biological control systems sensing or feeling the air around their wings[10]. Pressure measurement could be readily applied to a rigid wing MAV system with the use of common micro pressure transducers. As MAV systems need to be lite and small in design, sensing pressure around most of the wing would be unlikely. Placement of few pressure taps linking to a small pressure transducer system could be allow of an input to an autopilot system as appose to common IMU sensing system.

2 Experiment setup and pressure tap locations

2.1 Wing and experimental conditions

A NACA2313 wing was manufactured using CNC machinery methods and was reinforced by carbon fiber spars. The wing possessed 4 pressure insert modules manufactured by rapid prototyping methods (fig 1).

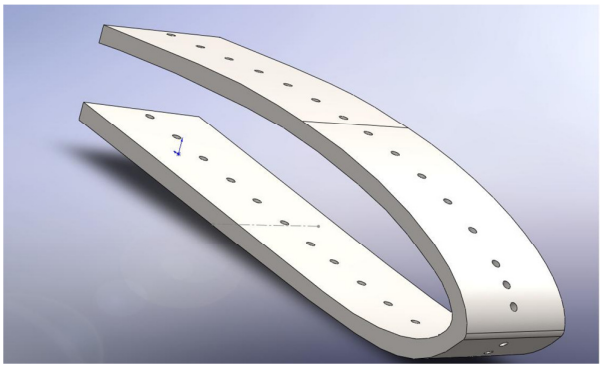

Figure 1: Design of pressure tap insert module allowing for PVC tube connections to pressure measurement device

The modules where placed at 4 span wise locations on the wing allowing PVC connections to dynamic pressure measurement system (fig 2).

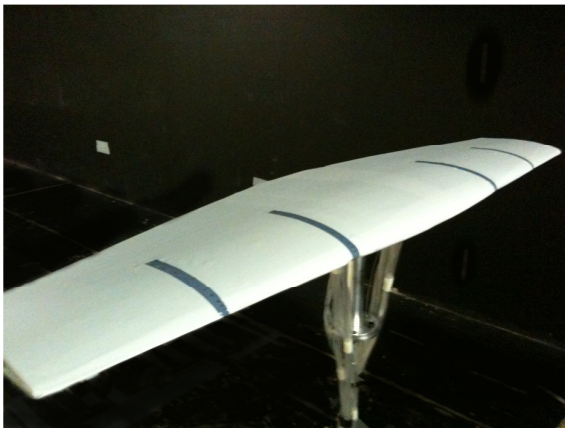

Figure 2: Manufactured NACA 2313 wing featuring pressure insert modules at 4 span wise locations.

The location of each tap features in table 1. Taps near the leading edge where manufactured closer together to ensure data resolution around the critical lifting region of the chord.

Pressure tap	NACA2313 (x/c) %
1	1.04
2	3.13
3	5.21
4	9.38
5	13.54
6	17.71
7	26.04
8	34.38
9	42.71
10	50.21

Table 1: Non-dimensional pressure tap locations for each wing insert module.

Pressure taps existed between 1 – 50% of the average chord as thinning towards the trailing edge inhibited installation of pressure taps. Span wise modules are symmetrical around the center line of the wing. The inboard and outboard modules are situated 166.7mm and 333.3 mm from the wing centerline on both wing semi-spans to allow for the application of strip theory with equal strip portions (see figure 2).

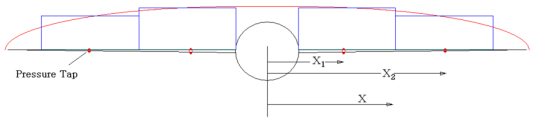

Figure 3: Span-wise pressure module placement for equal portion application of strip theory

Experiments where performed in the Royal Melbourne Institute to Technology (RMIT) industrial wind tunnel featuring a 3 x 2 x 9m test section. Smooth flow configuration produced nominal smooth-flow conditions of 1.2% Turbulence Intensity (Ti). A higher Ti was generated by grids placed before the contraction of the tunnel producing 7.2% Ti with integral length scale of approximately 0.23m measured by a 4 hole pressure-sensitive cobra probe provided by Turbulent Flow Instrumentation (TFI). Such conditions where generated to replicate a turbulence condition similar to atmospheric conditions MAVs fly within [14]. The NACA2313 wing was placed 9 meters downstream of the turbulence generating grids to allow for sufficient flow mixing for homogeneous freestream turbulence. Smooth and turbulent flow experiments where conducted at a freestream velocity of 8ms-1. Angles of attack raged from 0 to 20 degrees with a 5 degree step size.

2.2 Instrumentation

The Dynamic Pressure Measurement System (DPMS) used for experiments was manufactured by TFI allowing for high frequency data acquisition of dynamic pressure. Data acquisition was performed for all experiments at a rate of 2kHz for 300 seconds. A low pass filter of 100Hz cut-off frequency was applied post processing to eliminate effects of data aliasing. As this work focuses on oscillation frequencies below 50Hz the temporal and phase offset produced by system multiplexing was measured and concluded to be insignificant and neglected from results. The TFI software allows for a post processing routine to calibrate frequencies that are amplified or attenuated by the interconnecting PVC tubes [15].

3 Mean and standard deviation of surface pressures

3.1 Smooth flow condition

The mean and standard deviation of pressure co-efficient was calculated by the following equations.

$$C_p' = \frac{P' - P_\infty}{\frac{1}{2}\rho V^2} \quad (1)$$

$$C_p = \frac{P - P_\infty}{\frac{1}{2}\rho V^2} \quad (2)$$

Where: Cp and Cp' are the mean and transient pressure coefficients respectively, P

and P' are the mean and transient local pressures respectively, P_∞ is the ambient static pressure, ρ is density of air and V is the mean freestream velocity. The P_∞ was estimated by acquiring pressures from the static port of a Pitot-Static tube placed at the location of airfoil testing.

Evaluation of the mean pressure co-efficient over the measured surface of the NACA2313 wing displayed predictable profiles (fig 5). Results displayed focuses on the inboard wing pressure insert module on a single semi span.

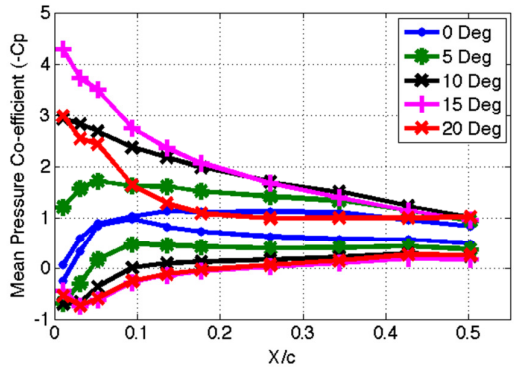

Figure 4: Mean pressure co-efficient of NACA2313 wing in nominally smooth flow (Ti = 1.2%, Lxx = 0.23m)

High suction occurred near the leading edge of the wing with gradual pressure recovery. Attached flow occurred at AOA between 0 and 15 degrees with flow separation evident at 20 degrees.

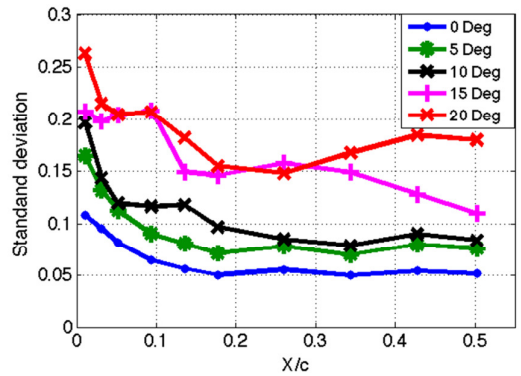

Figure 5: Standard deviation of pressure co-efficient under nominally smooth flow (Ti = 1.2%, Lxx = 0.23m)

Standard deviation of pressure co-efficient revealed increasing standard deviation as AOA increased when exposed to a smooth flow tunnel configuration (fig 6). Maximum variance occurs at the leading edge of the wing for all angles of attack. AOA of 0 and 5 degrees display a gradual reduction of pressure variance from leading edge to trailing edge while greater AOA display instabilities indicated by standard deviation spikes around 10% chord. Such instabilities have been found on similar low Reynolds number experiments which indicate formation of a laminar separation bubble and location of flow reattachment at the standard deviation peaks [16].

3.1 Turbulent flow condition

Turbulent flow conditions (Ti = 7%, Ixx = 0.23m), the mean suction over the airfoil was considerably different comparing smooth flow results (fig 7).

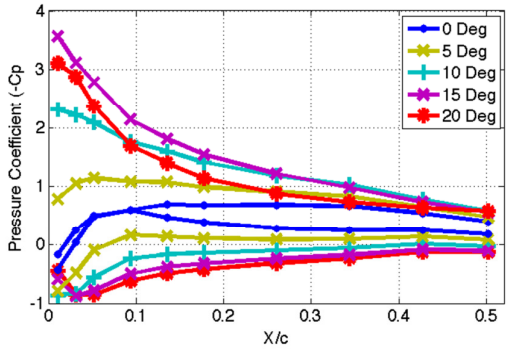

Figure 6: Time-averaged pressure co-efficient of NACA2313 wing under turbulent flow condition (Ti = 7.2%, Ixx = 0.23m)

Turbulent flow increased wing performance as flow separation is delayed mostly indicated by 20 degrees AOA offering a higher Cp profile.

The standard deviation of pressure co-efficient also displays contrasting results to smooth flow condition (fig 7).

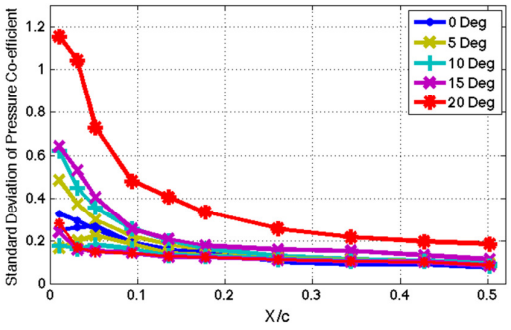

Figure 7: Standard deviation of pressure co-efficient in turbulent flow (Ti = 7%, Lxx = 0.23m)

Unlike smooth flow results, the standard deviation of pressure co-efficient for each angle off attack features maximum pressure variance at the leading edge of the wing without presence of pressure variance peaks for AOA above 5 degrees. Furthermore no peaks are observed indicating no laminar separation bubble formation. Pressure variance is also seen to increase as AOA increases. Specifically focusing on AOA of 20 degrees, standard deviation amplifies at all chord locations.

3 Relationship between local pressures tap and integrated chord-wise pressures

A cross correlation between time varying local pressures and integrated pressure was performed to qualify relationship for all angles off attack (fig 9).

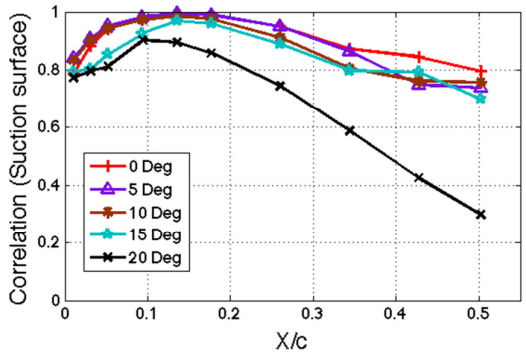

Figure 8: Correlation between local chord-wise pressure and integrated pressure on suction surface in turbulent flow.

Maximum correlation existed at x/c of 14% for angles of attack between 0 and 15 degrees (see figure 8). Furthermore angles of attack below 20 degrees suggest likeness with similar correlation co-efficient. It is evident that flow separation and 20 degrees AOA, (found in figure 6 and 7), reduces correlation between local and integrated Cp.

The pressure surface displayed contrasting correlation to chord location profiles featured in figure 9.

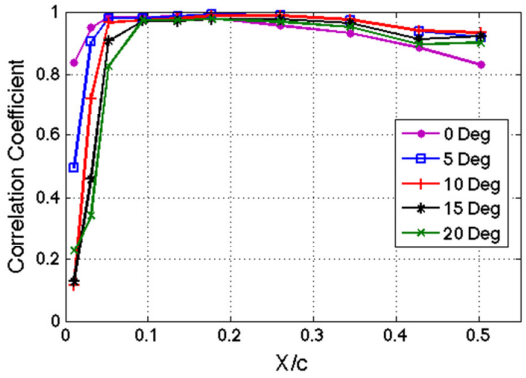

Figure 9: Correlation between local pressure and integrated Cp on pressure surface in turbulent flow.

Maximum correlation existed at 17% chord for all angles of attack with subtle reductions near the leading edge as angles of attack increased. Unlike the suction surface, no significant reduction in correlation is observed most notably at 20 degrees AOA as favorable pressure exists under all AOA tested.

The discovery of high correlation between local pressure to integrated Cp at 14% (suction surface) and 17% (pressure surface) chord did not show any obvious connection to the time-averaged pressure (fig 6) nor the standard deviation of pressure (fig 7). Interestingly enough the max correlation on suction and pressure surface occurred immediately after the maximum thickness of the airfoil suggesting connection to airfoil geometry rather than the pressure profile or pressure variance. Different maximum correlation locations between suction and pressure surface is assumed to be due to 2% camber of the airfoil.

Comparing the inboard and outboard pressure modules on a semi span did not yield significant change in max correlation location shown in figure 10 for AOA of 5 degrees.

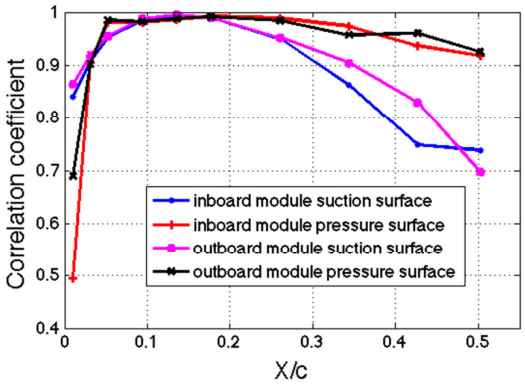

Figure 10: Correlation between local and integrated Cp for outboard and inboard pressure modules in turbulent flow at 5 degrees AOA.

Outboard pressure module located 333.3mm from wing centerline held likeness to inboard pressure module located at 166.7mm from wing centerline. Such observations suggesting wing tip vortices held insignificant influence on maximum correlation location and co-efficient value. This finding held true for all angles off attack.

4 Linear relationship between local and integrated pressure.

The correlation analysis identified a specific chord-wise location where local pressure and integrated Cp are linearly related and can be expressed as:

$$\int Cp \propto Cp_{local} \qquad (3)$$

Identifying the linear link between the two variables was performed by plotting time varying local pressure at 14% chord against time varying integrated Cp (fig 11).

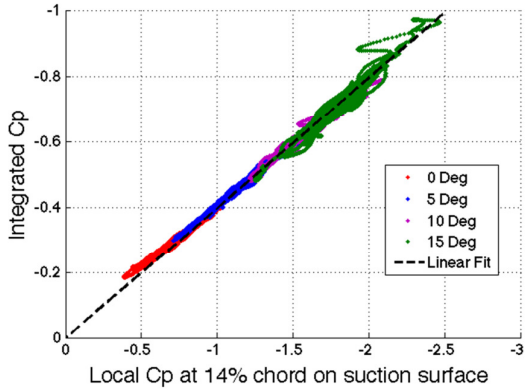

Figure 11: Scatter plot of time-varying integrated Cp and Cp at 14% chord on the suction surface of the inboard pressure module in turbulent flow.

The lift fluctuations at different AOAs occur sequentially with some overlap due to the variance in relative angle of attack of the oncoming freestream turbulence. The data scatter offers small deviation from best line of fit. Furthermore, small degree of scatter links well with the high correlation co-efficient discovered in figure 8 as the degree of linearity is relative to the square of correlation co-efficient. A subtle increase in scatter features in 15 degrees AOA as flow instability and separation occurs. Full separation occurs at 20 degrees AOA producing high data scatter and effectively delinearizating relationship between local and integrated Cp and is not featured in figure 11. Time averaged results linking integrated pressure to local pressure exposed linearity between the two variables for suction and pressure surface of the airfoil surface (fig 12).

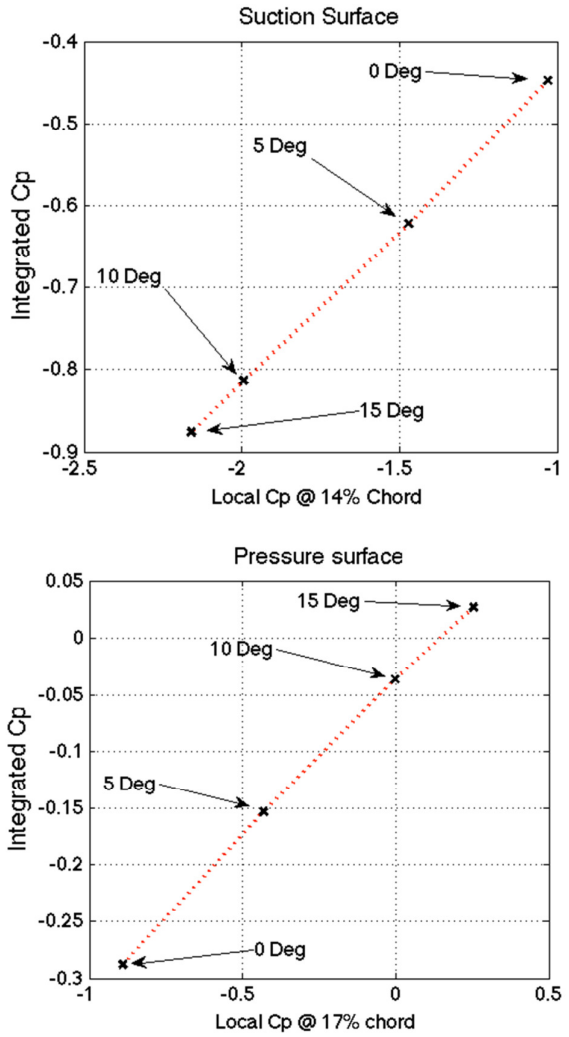

Figure 12: Linear relationship between integrated Cp and local Cp at 14% and 17% chord for the suction and pressure surface respectively for NACA2313 wing in turbulent flow (relating to inboard pressure module).

Linearity between local and integrated Cp for inboard pressure module can be expressed as:

$$\int Cp \approx 0.378 Cp_{local} \text{ (Suction Surface)} \quad (4)$$

$$\int Cp \approx 0.276 Cp_{local} \text{ (Pressure Surface)} \quad (5)$$

This analysis shows that one pressure tap located at a specific chord-wise location holds enough correlation to integrated Cp allowing for a single pressure tap to be used to estimate the time-varying lift at that section. If single pressure taps exist on the suction and pressure surface at various span wise section of a wing, strip theory used by resolving the lifting vector at each span wise section to gather real time measurement of roll and lift in flight.

5 Conclusions

The discovery of a local chord-wise location, which linearly correlates to integrated pressure, displays no obvious relationship to time-averaged Cp profiles nor pressure variance on the suction and pressure surface of the wing. Maximum correlation featured after the maximum thickness of the wing indicating a possible reliance on geometric airfoil parameters. Furthermore, under attached flow conditions a linear relationship exists while flow detachment breaks down relationship resulting in a limitation to the discovery. By implementing a single pressure tap to the suction and pressure surface at various span-wise sections, strip theory can be applied to resolve for lift and roll in real time. Pressure sensing as an input to an autopilot system may be an advantageous method for turbulence mitigation as the disturbance is sensed before aircraft perturbation as apposed to an IMU sensing a perturbation that has already affected flight. Future comparison studies between IMU and pressure sensing may be key in concluding pressure sensing to hold a time forward prediction of aircraft turbulence response.

5 References

[1] J. L. Palmer, "Aerodynamic and Performance Characteristics of Small Unmanned Aerial Vehicles Compared with those of Manned Aircraft," Defence Science and Technology Organisation, Melbourne, Australia2009.

[2] J. M. McMichael and C. M. S. Francis, "Micro Air Vehicles - Toward a New Dimension in Flight," DARPA, USA1997.

[3] H. Chao, Y. Cao, and Y. Chen, "Autopilots for Small Fixed Wing Unmanned Air Vehicles: A Survey," in *Mechatronics and Automation, 2007. ICMA 2007. International Conference* Harbin: Utah State University, 2007, pp. pp. 3144-3149.

[4] S. Watkins, J. Millbank, and B. Loxton, "Atmosheric Winds and their Effects on Micro

Air Vehicles," *AIAA Journal of Aircraft,* vol. v. 44, 2006.
[5] A. S. Wu, A. C. Schultz, and A. Agah, "Evolving Control for Distributed Micro Air Vehicles," in *Computational Intelligence in Robotics and Automation, 1999. CIRA '99. Proceedings. 1999 IEEE International Symposium* Monterey, CA, USA, 1999, pp. pp. 174-179.
[6] J. William R. Davis and B. B. Kosicki, "Micro Air Vehicles for Optical Surveillance," *The Lincon Laboratory Journale,* vol. Vol. 9, pp. pp. 197-213, 1996.
[7] M. A. S. Watkins, M. Thompson, M. Shortis, R. Segal and J. Sheridan "An Overview of Experiments on the Dynamic Sensitivity of MAVs to Turbulence " 2010.
[8] M. Abdulrahim, S. Watkins, R. Segal, M. Marino, and J. Sheridan, "Dynamic Sensitivity to Atmospheric Turbulence of Unmanned Air Vehicles with Varying Configuration," *Journal of aircraft,* vol. 47, pp. 1873 - 1883, 2010.
[9] B. W. Tobalske, "Biomechanics of bird flight," *The Journal of Experimental Biology,* vol. 210, pp. 3135 - 3146, 2007.
[10] S. Dhawan, "Bird flight," *Sadhana,* vol. 16, pp. 275-352, 1991.
[11] A. L. R, T. Taylor, and G. K. Taylor, "Animal Flight Dynamics I. Stability in Gliding Flight," *Journal of Theoretical Biology,* vol. Vol. 212, pp. pp. 399-424, 7 October 2001 2001.
[12] M. Abdulrahim, H. Garcia, J. Dupuis, and R. Lind, "Flight Characterictic of Wing Shaping for a Micro Air Vehicle with Membrane Wings," University of Florida2004.
[13] G. C. H. E. d. Croon, K. M. E. d. Clercq, R. Ruijsink, B. Remes, and C. d. Wagter, "Design, aerodynamics, and vision based control of the Delfly," *International Journal of Micro Air Vehicles* vol. 1, pp. 71-97, 2009.
[14] J. Millbank, B. Loxton, S. Watkins, and W. H. Melbourne, "Replication of Atmospheric Conditions for the Purpose of Testing MAVs," Royal Melbourne Institute of Technology, Melbourne, Australia23 DEC 2005 2005.
[15] H. Berge and H. Tijdemen, "Theoretical and experimental results for the dynamic response of pressure measuring systems," National Aerospace Laboratories1965.
[16] T. J. Muller and J. D. DeLaurier, "Aerodynamics of Small Vehicles," *Annual Review of Fluid Mechanics,* vol. Vol. 35, pp. pp. 89-111, January 2003 2003.

Copyright Statement